Ultrafast Pump-Probe Experiments with an Exemplar Biomolecule, Phenylalanine.

Contact *lbelshaw01@qub.ac.uk, j.greenwood@qub.ac.uk*

L Belshaw, CR Calvert, MJ Duffy, O Kelly, RB King, AG Smyth, ID Williams, and JB Greenwood.

Centre for Plasma Physics
School of Mathematics and Physics
Queen's University Belfast

WA Bryan,

Department of Physics, Swansea University

T. Kierspel, P. Rice, ICE Turcu, CM Cacho and E Springate

Central Laser Facility, STFC, Rutherford Appleton Laboratory

Introduction

Ultrafast charge transfer in biomolecules is believed to be at the heart of a number of important biological processes, for example vision, ultraviolet DNA damage and light harvesting in photosynthesis. A number of theoretical studies on peptides which contain one or more amino acids with a chromophore site predict fast charge migration across the molecule on a period of a few femtoseconds or less (1). On such timescales, short pulse laser systems provide the perfect tool for resolving or influencing the dynamics, as has been shown for atoms and diatomic molecules (see for example (2) and references therein). Phenylalanine (Phe) is a candidate molecule with which to investigate these ultrafast processes in larger, biomolecular systems, as its radical cation possesses two charge sites with similar energies which could potentially act as donor or acceptor sites; the phenyl ring side chain and the amine site. Experimental observations of a derivative molecule, 2-phenylethyl-N,N-dimethylamine, indicated downhill charge transfer via a conical intersection from the aromatic ring to the methylated amine group in 80 fs (3). It is noteworthy that in this study, a few-fs process would have been outside of the resolution of the experiment, undertaken with pulse durations on the order of 100 fs. Meanwhile recent theoretical calculations on another related molecule, 3-methylen-4-penten-N,N-dimethylamine, demonstrated charge oscillations with a period of 4 fs (4). In this report we present a pump-probe study of Phe using pulses which are shorter than the fastest vibrational periods in the molecule (<10 fs). While our results indicate that the fragmentation mechanisms proceed on much longer timescales and hence we were unable to observe any ultrafast charge transfer, we have demonstrated such experiments are feasible and that two colour pump-probe experiments in the future could facilitate such observations.

Experimental Technique

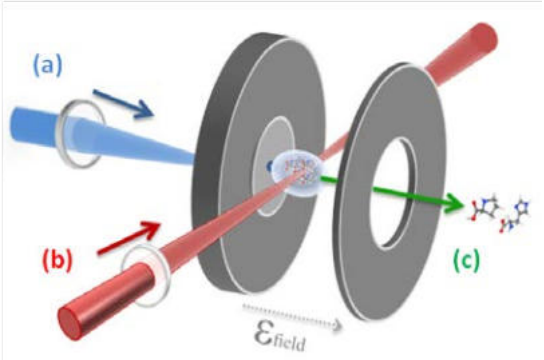

Figure 1: Schematic diagram of LIAD-fs; A UV, ns laser pulse irradiates the reverse side of a thin Ta foil, generating a plume of neutral biomolecules in the gas phase (a). This is crossed with a fs laser (b), and resulting ions are extracted by an electrostatic field and analysed in a time-of-flight device (c).

Preparing a biomolecular target in the gas phase allows single molecules to be studied free from the influence of solvents or their surrounding environment. A number of techniques for generating molecules in the gas phase have been developed, including matrix-assisted laser desorption/ionisation and electrospray (5). This report will discuss the relatively new method of laser-induced acoustic desorption (LIAD) (6). Unlike other techniques, LIAD produces neutral molecules, and does not require direct laser radiation of the sample. It also does not involve the addition of a so-called matrix molecule, which can yield spurious signal in the resulting mass spectra.

In our scheme, LIAD involves the deposition of a biomolecular sample onto one side of a thin (10 μm) tantalum foil. The foil is subsequently irradiated from the rear side with a ns, UV (355 nm), laser pulse. The resultant shock wave initiated in the foil liberates the molecules from the front surface of the foil, forming a gas phase plume of neutral and intact biomolecules. The plume is then crossed with a fs laser pulse, delayed from the LIAD generation pulse by approximately 20 μs, and the resulting ions are extracted with an electrostatic field and analysed in a time-of-flight device (see figure 1 for a schematic). LIAD-fs has been characterised in detail, and a full description can be found elsewhere (7).

All experiments were performed using the Artemis Laser at the Central Laser Facility (8). Pulses of duration 30 fs were compressed to <10 fs using a series of chirped mirrors following propagation through a hollow fibre, after which the energy was typically on the order of 0.5 mJ.

Ultrafast Pump-Probe Setup

The target plume of molecules generated by LIAD is probed by two laser pulses of fs duration, central wavelength λ = 790 nm, delayed in time by τ_D. These two fs pulses are generated in a Mach-Zehnder interferometer by splitting the initial beam into two components; one of which is subsequently delayed with respect to the other by increasing its path length. The first pulse serves to ionise the molecules, and the second pulse to probe the ions which remain.

In order to find the temporal window in which the two pulses are overlapped, and thus determine the time delay between the pulses, xenon was introduced into the interaction region of the time-of-flight spectrometer through a needle valve – generally increasing the pressure from a background value of 10^{-8} mbar to 10^{-7} mbar. The ionisation yield of xenon can be observed to produce a typical autocorrelation signal, with the maximum signal corresponding to complete overlap of the two pulses and, therefore, time-zero. An example autocorrelation of Xenon is shown in figure 2, in which the pulses were split in a 60/40 beam splitter. From this signal, it is possible to extract the original pulse duration – for example, a pulse duration of τ_L = 8.5 ± 1.0 fs in figure 2 was obtained by observing the autocorrelation of all the isotopes of xenon and also of background signal from H_2O present in the vacuum chamber.

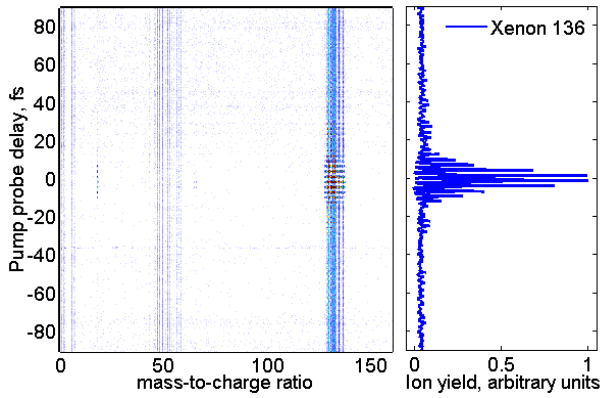

Figure 2: (a) Autocorrelation signal of xenon. The two pulses were generated with a 70/30 beam splitter, yielding on-focus intensities of I = 1.0 x 10^{13} Wcm^{-2} and I = 2.6 x 10^{13} Wcm^{-2}. (b) Integrated ion yield from an isotope of xenon; from studying signal of xenon isotopes and water, the pulse duration was determined to be 8.5 ± 1.0 fs.

Results and Discussion

It is helpful for the discussion to first observe the mass spectrum produced with a single fs pulse used to ionise the target plume, with pulses of central wavelength 790 nm, on-focus intensity 3.5 x 10^{13} Wcm^{-2}, and pulse duration 20 ± 2 fs, measured using a third-order autocorrelator (FROG). Phe, which has a parent mass of 165 amu, is sketched in the inset of figure 3(a). Four main fragments, plus the parent ion, can be identified in this spectrum. The fragments located at mass to charge ratios of 120 and 74 arise from an alpha-cleavage mechanism following charge residing on the NH_2 group, whereas the peaks at 91 and 92 follow bond breakage from charge located in the phenyl group (9).

With an understanding of the fragmentation following ionisation in a single pulse study, we can begin to study dynamics. Movement of charge within the molecule should manifest itself as a variation of the yield of the mass peaks with respect to time. A number of pump-probe studies were undertaken on Phe; a typical result from these studies is illustrated in figure 3. For this particular example, the two fs pulses had pulse durations of 10.0 ± 1.5 fs (determined using an autocorrelation of xenon, as discussed above), and energies of 0.11 and 0.08 mJ. Focussing using a spherical mirror to the interaction region yielded peak intensities of 2.5 x 10^{13} and 9.9 x 10^{12} Wcm^{-2} at a point 2mm from focus. The pump-probe delay, τ_D, was varied from -100 to + 100 fs, with a step size of 3.33 fs.

The first thing of note is that the key fragments of the spectra are the same as those observed from a single pulse study (see figure 3(a). A number of low mass fragments (below m/q = 70 amu) are also visible; these are simply due to the relatively high intensity of the laser pulses used causing the molecule to fragment more completely, and also from background gases in the vacuum chamber, such as H_2O and N_2.

Over the time period studied, no variations in relative mass yields can be observed. For example, in figure 3(b) (bottom), the integrated ion yield from water present in the vacuum chamber is plotted as a lineout, clearly illustrating increased ion production at time-zero. In 3(b) (top), the ratio of two fragment mass peaks arising from phenylalanine is plotted, that of m/q = 91 to m/q = 92. Taking a ratio of the two allows the influence of any shot-to-shot variation inherent in the LIAD technique to be minimised. It can be observed that any variations appear consistent with those in the ionisation yield of water.

Overall, it seems that the spectra are arising from a summation of the contributions from the two pulses individually, indicating that the fragmentation is proceeding more slowly than 100 fs, or the charge transfer is too rapid to be resolved with the current pulses which are on the order of 10 fs.

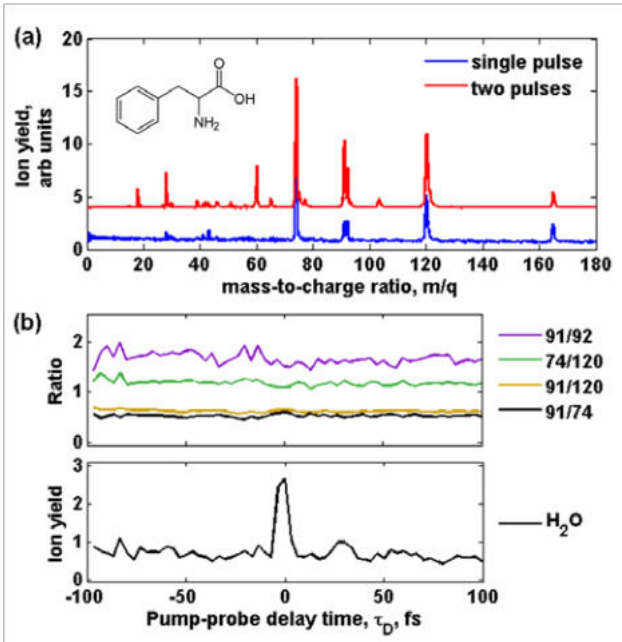

Figure 3: (a) The mass spectrum produced by photoionisation of Phe (inset), with a single pulse (blue); and the typical mass spectra observed during a two pulse study (red, τ_D = 0 fs), this plot is offset in the y direction from zero for clarity.
(b) Integrating the ion yield of a particular mass at each pump-probe delay time, τ_D. Top: Ratios pertinent to charge migration in Phe, notated in the legend; and bottom: ionisation yield of H_2O, clearly indicating t_0.

Conclusions

Although no evidence for ultrafast charge transfer has been observed here in the molecule Phe, it has been demonstrated that ultrafast pump-probe studies in such complex molecules are possible. This is the first such study in larger molecules, and the feasibility of such an approach is shown. In future, a two colour experiment, where the pump pulse clearly localises the initial charge site through resonantly enhanced multi photon ionisation, could prove more successful. This would not only define the initial ionisation site, but also reduce fragmentation from the pump pulse allowing the individual effects from the pump and probe pulses to be identified.

Acknowledgements

LB and MJD acknowledge funding from the Department of Employment and Learning, Northern Ireland. CRC acknowledges funding from the EPSRC through a Postdoctoral Fellowship at the Physics – Life Sciences Interface, and OK and RBK from the Leverhulme Trust.

References

1. R. Remacle and D. Levine *PNAS* **103**, 6793 (2006).
2. C.R. Calvert, W.A. Bryan, W.R. Newell, and I.D. Williams *Physics Reports* **491**, 1 (2010).
3. L. Lehr, T. Horneff, R. Weinkauf, and E.W. Schlag *J. Phys. Chem. A* **109**, 8074 (2005).
4. S. Lunnemann, A.I. Kuleff, and S. Cederbaum *J. Chem. Phys.* **129**, 104305 (2008).
5. K. Tanaka *et al Rapid. Commun. Mass Spectrom.* **2**, 151 (1988); J.B. Fenn *et al Science* **246**, 67 (1989).
6. V.V. Golovlev, S.L. Allman, W.R. Garrett, N.I. Taraneko, and C.H. Chen *Int. J. Mass Spectrom. Ion Processes* **169-170**, 69 (1997).
7. C.R. Calvert *et al Phys. Chem. Chem. Phys.* **14**, 6289 (2012).
8. ICE Turcu *et al Proc. SPIE* **7469**, 746902 (2010).
9. V. Vorsa, T. Kono, K.F. Willey, and N. Winograd *J. Phys. Chem. B* **103**, 7889 (1999).

Towards UV pump XUV probe photoelectron spectroscopy of chemical dynamics

Contact *r.s.minns@soton.ac.uk*

R.S. Minns

Chemistry, University of Southampton,
Highfield Campus, Southampton, SO17 1BJ

R. Spesyvtsev and H.H. Fielding

Department of Chemistry, University College London, 20 Gordon St, London WC1H 0AJ

D.J. Hadden, S.E. Greenough and V.G. Stavros

Department of Chemistry, University of Warwick
Coventry, CV4 7AL

D.A. Horke

Department of Chemistry, Durham University
Durham, DH1 3LE

J.G. Underwood

Department of Physics, University College London
Gower Street, London, WC1H 6BT

S. Weber, M. Siano and J. Marangos

Department of Physics, Imperial College London
London, SW7 2 AZ

D.M.P. Holland

Photon Science Department ,STFC Daresbury Laboratory,
Warrington WA4 4AD

I.C.E. Turcu, C.E. Caucho and E. Springate

Central Laser Facility, STFC Rutherford Appleton Laboratory
Didcot, UK

Introduction

The development of femtosecond x-ray sources is set to revolutionize atomic, molecular and optical science. The areas covered are as diverse as single shot diffractive imaging of gas phase biomolecules[1] to highly non-linear ionisation dynamics of noble gases[2]. Both of these examples rely not only on the ultrashort pulse durations but also the remarkably high intensities that are now available at fourth generation light sources. Another route to femtosecond extreme ultraviolet (XUV) and soft x-ray light is the laboratory based technique of high harmonic generation (HHG). In these sources the ionisation, acceleration and subsequent re-collision of an electron from a noble gas leads to the emission of a highly energetic photon on a femtosecond or even sub-femtosecond timescale. The femtosecond duration of the light source lends itself to the grand challenge of understanding chemical reactivity and molecular dynamics which occur on this fundamental timescale.

The study of photoinduced molecular dynamics is really concerned with the non-adiabatic interactions that couple vibrational and electronic degrees of freedom and control the majority of photochemical reactions in physics, chemistry and biology. A key tool for following these dynamics is time resolved photoelectron imaging (TRPEI) through which it is possible to instantaneously measure the electronic and nuclear configuration of a molecule over the course of a reaction. The basic concept of TRPEI is that a chemical event is triggered with an ultrashort laser pulse (pump) and is subsequently ionised with a second delayed laser pulse (probe) at a number of different delays after excitation. The energies and angular distributions of the outgoing electrons are subsequently measured and the dynamics of the system are inferred from changes in the measured photoelectron image. In most cases it has not been possible to ionise the entire reaction coordinate due to the large ionisation limits of some reactive intermediates and products. This leads to significant blind spots in the reaction mechanism where no information about the system is obtainable. The limiting factor has been the wavelength range over which conventional femtosecond lasers can work. A potential solution to this limitation is to use ultrafast XUV photons generated via HHG as the probe. The experiments described below outline the first steps towards using XUV light from a HHG source for time resolved photoelectron imaging experiments at the Artemis laser facility

Experimental details and development

The experiments make use of many of the capabilities at Artemis including: an optical parametric amplifier for the generation of UV pump pulses, a high harmonic generation source and monochromator for the probe and a velocity map imaging (VMI) spectrometer.

The pump and probe pulses are generated from the 1 kHz, 30 fs, 780 nm output from the Red Dragon laser system. 8 mJ are used to pump the high energy OPA (TOPAS) to produce approximately 10 μJ UV light at ~240 nm to act as the pump.

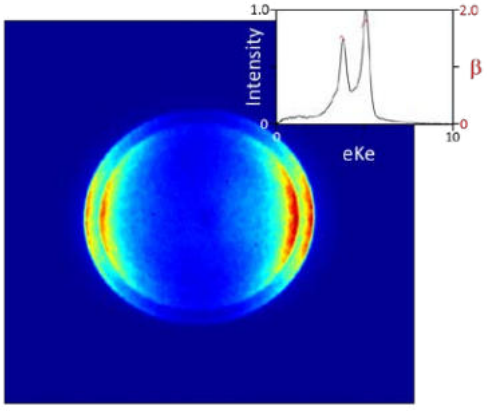

Figure 1. Photoelectron image of Xe taken with the 11th harmonic. Inset: retrieved photoelectron spectrum obtained via the Polar Onion Peeling algorithm.

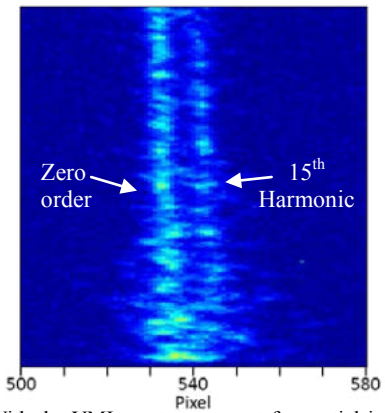

Figure 2. With the VMI spectrometer set for spatial imaging the shift in position of the harmonics in the plane of the detector can be seen as the grating is tuned from zero order to the 15th harmonic.

The probe was generated via HHG of the fundamental using approximately 1 mJ of the output of the Red Dragon focused into a gas jet of Ar. The 780 nm driving field and the harmonics produced are passed into the time preserving monochromator[3] which spatially separates each of the harmonics. By tuning the monochromator grating angle a single harmonic can be selected which is focused into the interaction region of the VMI chamber with a torroidal mirror. The source provided a harmonic flux on the order of 10^6 photons per second per harmonic for harmonics 11 to 23. The pump and probe pulses were then crossed in the centre of the interaction region at a small angle (~1°). The primary step was to attach the AMO chamber to the end of the monochromated beamline and obtain images for some simple gas targets. To this end we collected several images for different harmonics to calibrate the detector and measure signal levels. Several images were taken at various harmonics for calibration and characterization purposes (figure 1). In order to obtain a pump-probe signal initial overlap utilized the residual IR driving field that passes through the monochromator when it is at zero order. The method used involved tuning the TOPAS to a long lived state in Xe (a two photon resonance at 255 nm was used) from which the IR could ionize Xe with the absorption of another photon. As the UV pulse was tuned to a long lived resonance as the time delay between the two pulses was scanned a clear step in the Xe ion or photoelectron signal was observed.

The monochromator is designed such that adjusting the grating to tune to a particular harmonic should not move the beam. However, this turned out not to be the case and a small but significant shift in the beams was observed (figure 2) and while the deviation could be measured in the plane of the detector it remained unknown in the other dimension. This has led to the installation of a new beam profiling crystal that will allow for the direct imaging of the XUV and UV beams in situ. This removes the uncertainty in the relative beam positions and should allow optimization of the overlap without having to adjust on the small pump probe signals that are expected. It will also provide a measure of the XUV and UV focal spot sizes.

The uncertainty in the overlap limited what was possible in terms of obtaining a pump probe signal. While a UV pump XUV probe signal was observed at zero order no such signal was observed once the harmonics has been monochromated.

Other developments have been towards increasing the photon flux from the HHG source. This will include the installation of an extended gas cell and longer focal length lens to increase the interaction length maximizing the harmonic flux.

Conclusions

A series of experiments have been performed to investigate the possibility of performing UV pump XUV probe experiments at the Artemis laser facility. While these experiments have not been successful so far some key areas that require development for these experiments have been identified and are now actively being improved. A new set of experiments to test these developments and the potential for UV pump XUV probe photoelectron spectroscopy are due to get underway in July 2012.

Acknowledgements

RSM thanks the Ramsay trust for a fellowship. HHF and RS are grateful to the European Marie Curie Initial Training Network Grant No. CA-ITN-214962-FASTQUAST for a studentship (RS). S.E.G and D.J.H. thank the EPSRC for doctoral training studentships. V.G.S thanks the Royal Society for a University Research Fellowship.

References

1. H. N. Chapman*, et al.*, Nat. Phys. 2, 839, 2006.
2. H. Wabnitz*, et al.*, Nature 420, 482, 2002.
3. F. Frassetto *et al*. Opt. Exp. **19** 19169 (2011)

Coherent collective-mode oscillations in the $K_{0.3}MoO_3$ charge density wave[1]

Contact *j.petersen1@physics.ox.ac.uk*

JC Petersen, A Cavalleri

Dept. of Physics, Oxford University, Clarendon Lab., Oxford
Max Planck Group for Structural Dynamics, CFEL, University of Hamburg

HY Liu, I Gierz, S Kaiser, A Simoncig, AL Cavalieri

Max Planck Group for Structural Dynamics, CFEL, University of Hamburg

C Cacho, ICE Turcu, E Springate

Central Laser Facility, STFC Rutherford Appleton Laboratory

F Frassetto, L Poletto

LUXOR, CNR-INFM, Padova, Italy

S Dhesi

Diamond Light Source Ltd.

Z-A Xu

Department of Physics, Zhejiang University, Hangzhou, China

T Cuk

Materials Science and Physical Biosciences Divisions, Lawrence Berkeley National Lab., Univ. of California, Berkeley

Introduction

The total energy of a low-dimensional metal can be lowered by a periodic distortion of the crystal lattice. This phenomenon, called a Peierls transition [2], enlarges the unit cell and redistributes charge density through electron-phonon coupling. One or more band gaps may then open, often causing a metal-to-insulator transition. Formation of such a charge density wave (CDW) ground state generates new low-energy collective excitations, distortions and translations of the charge density called amplitude and phase modes [3]. The amplitude mode is only weakly momentum-dependent, but the phase mode is an acoustic excitation, dispersing linearly near k=0.

Blue bronze, $K_{0.3}MoO_3$, has a linear chain structure (Fig. 1(a)). The electronic properties are quasi-one-dimensional, favoring Peierls physics. A CDW forms at 180 K, an electronic gap opens at the Fermi level [4], and the new collective modes appear in infrared, Raman and neutron spectra [5–11]. Here, using time- and angle-resolved photoemission spectroscopy (tr-ARPES) [12], we study the momentum-dependent electronic structure of blue bronze evolving in time after optical excitation, to understand how the collective modes couple to the band structure and to each other.

Methods

We use the tr-ARPES system at Artemis in the Central Laser Facility [13]. A 790 nm, 30 fs laser pulse is split into two. One stimulates the sample with a fluence of 0.5 mJ/cm^2. The other creates high harmonics in a gas jet in a vacuum beamline. 20.4 eV photons, selected by a grating monochromator, are focused onto the sample in UHV. Photoelectrons emitted after each UV pulse are collected and analyzed. Their energies and directions give the distribution, in energy E and momentum k, of the states that had been occupied in the material. Varying the pump-UV delay gives the time evolution through a photoinduced insulator-to-metal transition.

Results

Static photoemission (Fig. 1(b)) resolves four bands below E_F. These hybridized Mo-4d and O-2p states disperse in accord with calculation [14] and experiment [15–16]. Fig. 1(c) shows energy distribution curves (EDCs) at different k. At the Fermi momenta k_F^{B1} and k_F^{A2} the EDCs cross a single band, but those at k_F^{A1} and k_F^{B2} cross both a bonding and an anti-bonding band, resulting in double peaks.

After pumping, intensity shifts from the equilibrium bands to E_F (Fig. 2) as the CDW ground state melts into a transient metallic phase. Fig. 3 shows the time evolution, near E_F, at each k_F. The B1 band oscillates rapidly, and A2 more slowly. The B1 frequency, 1.7±0.2 THz, matches the coherent amplitude-mode oscillation seen in optical absorption [8], but now indicating also the position in k-space where that excitation acts. A2 oscillates at 0.8±0.2 THz. At k_F^{B2} and k_F^{A1}, EDCs contain both bonding and anti-bonding bands and both frequencies are seen.

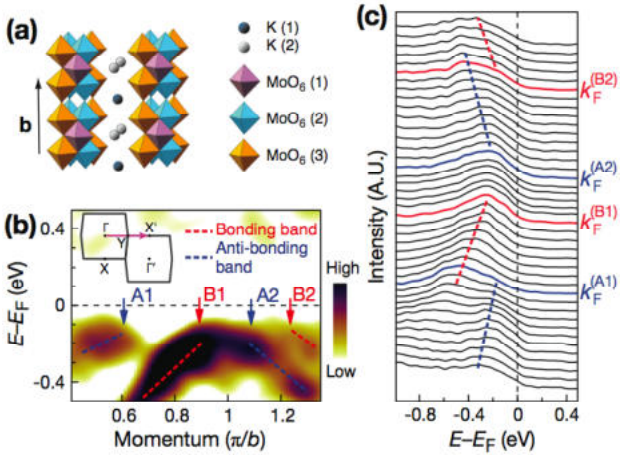

Fig. 1: Crystal structure (a) and photoemission band map (b) of blue bronze. Blue and red: anti-bonding (A1, A2) and bonding (B1, B2) bands. Fermi momenta, marked by arrows, are highlighted in the energy distribution curves (c). All measurements along the chain direction. In (b), d^2I/dE^2 is shown to highlight the underlying band structure.

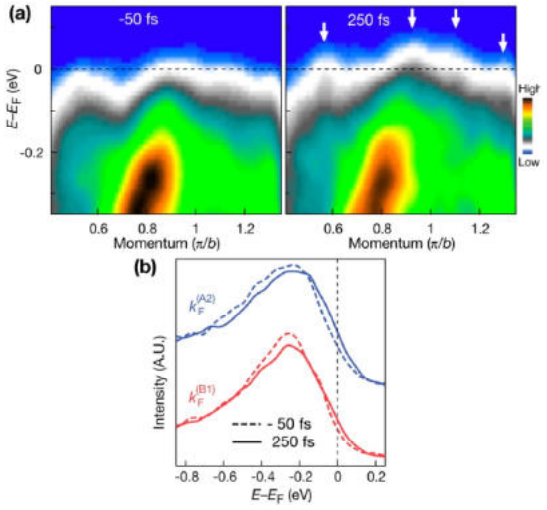

Fig. 2: Changes after photoexcitation. (a) Photoemission intensity at -50 and +250 fs (same color scale). Arrows show growth above E_F. (b) Transfer of states from conduction bands to E_F as the CDW gap melts.

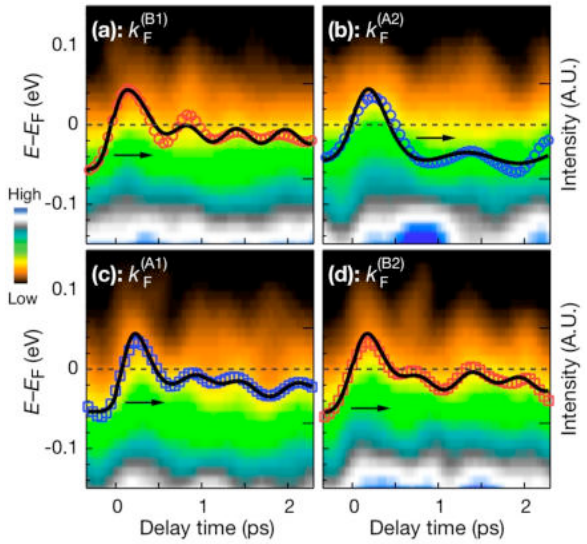

Fig. 3: Gap dynamics at the Fermi momenta. False-colour plots show intensity as a function of binding energy evolving in time. Symbols: integrated intensity from –50 to +100 meV. Solid lines: fits to decaying oscillations at 1.7 THz (a), 0.8 THz (b), or both (c,d).

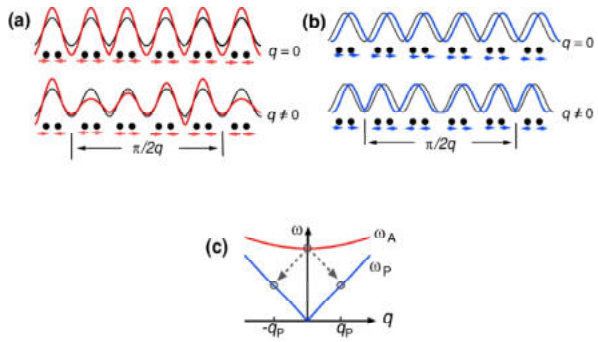

Fig. 4: Schematic representation of a CDW state in 1D. Dots represent atoms, arrows their displacements from the undistorted lattice points. Black lines: equilibrium charge density. Colored lines: Charge density modulated by an amplitude (a) or phase (b) mode. (c): Amplitude and phase mode dispersion, and the parametric phason generation process. Pinning or commensuration may gap the phase mode at q=0.

Discussion

The 0.8-THz oscillation must be the $q\neq0$ CDW phase mode, which varies from 0.1–1 THz [10,11], reaching 0.8 THz for $q_P=0.76b^*$ (with the reciprocal lattice constant $b^*=2\pi/b$). Suggestively, this equals the wave vector of the CDW itself, which nests the Fermi surface sheets of the anti-bonding and bonding bands.

In the linear regime, an optical pulse cannot excite the Raman-inactive phase mode directly, but strong pumping may drive some anharmonicity in the order parameter. Since the phase mode is driven at near half the amplitude-mode frequency, a single $q_A=0$ amplitudon might parametrically generate two phasons at $\pm q_P$ with energy $\omega_P(\pm q_P)=\omega_A(0)/2$, conserving energy and momentum (Fig. 4(c)).

This is the first direct observation of an impulsively excited coherent CDW phase mode. The coupling of the band structure to the collective excitations is momentum-selective, the bonding band being driven by the amplitude mode and the anti-bonding by the phase mode, which may relate to the bands' different orbital characters.

Conclusions

Using time- and angle-resolved photoemission spectroscopy at extreme ultra-violet wavelengths, we have investigated the momentum-dependent dynamics of the electronic structure of photo-stimulated blue bronze. After the CDW gap melts, an amplitude mode oscillation at 1.7 THz modulates the gap in the bonding band. More surprisingly, the anti-bonding band gap is instead modulated at 0.8 THz. We attribute this effect to the non-Raman-active CDW phase mode, coherently excited by anharmonic dynamics in the strongly driven order parameter.

References

1. H.Y. Liu *et al.*, arXiv:1206.5743 (2012)
2. R. Peierls. *Quantum Theory of Solids*. (Oxford University Press, 1955)
3. G Grüner. *Density Waves in Solids.* (Perseus, 2004)
4. G. Travaglini *et al., Solid State Commun.* **37** 599 (1981); D.C. Johnston, *Phys. Rev. Lett.* **52** 2049 (1984); R.S. Kwok *et al., Phys. Rev. Lett.* **65** 365 (1990)
5. G. Travaglini *et al., Solid State Commun.* **45** 289 (1983); D.M. Sagar *et al., New J. Phys.* **10** 023043 (2008)
6. Y.H. Ren *et al., J. Chem. Phys.* **120** 4755 (2004)
7. J. Demsar *et al., Phys. Rev. Lett.* **83** 800 (1999)
8. A. Tomeljak *et al., Phys. Rev. Lett.* **102** 066404 (2009)
9. H. Schäfer *et al., Phys. Rev. Lett.* **105** 066402 (2010)
10. J.P. Pouget *et al., Phys. Rev. B* **43** 8421 (1991)
11. H.K. Ng *et al., Phys. Rev. B* **33** 8755 (1986); G. Mihaly *et al., Phys. Rev. B* **39** 13009 (1989); B.P. Gorschunov *et al., Phys. Rev. Lett.* **73** 308 (1994)
12. L. Perfetti *et al., Phys. Rev. Lett.* **97** 067402 (2006); F. Schmitt *et al., Science* **321** 1649 (2008); J.C. Petersen *et al., Phys. Rev. Lett.* **107** 177402 (2011)
13. F. Frassetto *et al., Opt. Express* **19** 19169 (2011)
14. M. Whangbo and L. Schneemeyer, *Inorg. Chem.* **25** 2424 (1986); U.V. Waghmare *et al., Comput. Phys. Comm.* **137** 341 (2001); J. Mozos *et al., Phys. Rev. B* **65** 233105 (2002)
15. R. Claessen *et al., J. El. Spec. Rel. Phe.* **76** 121 (1995); B. Dardel *et al., Europhys. Lett.* **19** 525 (1992)

The commissioning of the AMO end station at Artemis: first steps toward Laser Induced Electron Diffractions

Contact *m.sianoo08@ic.ac.uk*

M. Siano, R. J. Squibb, M. Opperman, T. Siegel and J. P. Marangos

Q.O.L.S, Imperial College London
Blackett Laboratory, South Kensington Campus, London, SW7 2AZ

J. Underwood

Department of Physics, University College London
Gower Street, London, WC1H 6BT

I.C.E. Turcu, C.E. Caucho and E. Springate

Central Laser Facility, STFC Rutherford Appleton Laboratory
Didcot, UK

Introduction: Laser Induced Electron Diffraction (LIED)

When an atom or a molecule is subject to a strong laser field the potential barrier which keeps electrons bound to the parent ion is weakened. If the field intensity is high enough the tunnel effect can occur (tunneling ionization [1]) in which an electron is promoted into the continuum from the highest occupied molecular orbital. For electrons released into the continuum just after the peak of the electric field and for linearly polarized light it can be shown with very simple classical arguments that the electrons return on the parent ion around half a field cycle later. Consequently recollision with the parent ion can occur [2].

On recollision the electron can either recombine with the parent ion producing a burst of XUV photons (High Harmonic Generation) or can be rescattered, elastically or inelastically. In case of rescattering on a molecular ion the electron momentum distribution is expected to show an interference pattern due to the scattering on different centre. This effect is expected to be particularly clear for diatomic molecules for which the diffraction pattern is expected to be analogous to the one generated by the light propagating through a double slit. This effect has been named Laser Induced Electron Diffraction (LIED) and it has been theoretically predicted ([3],[4]) and observed experimentally ([5]). In this last work in the momentum distribution maxima and minima can clearly be seen, their position being related to the interatomic distance.

The original objective of the LIED experimental campaign at Artemis was to improve and extend the results of the work in [5] overcoming its main limitation which is its lack of scalability to larger molecules. The Artemis facility offers a great opportunity to achieve these results thanks to a newly designed high energy Velocity Map Imaging spectrometer and the capability to generate stable and intense laser pulses at wavelengths 1000 - 1600 nm and beyond.

Employing a longer wavelength with respect to [5] would make the diffraction pattern clearer and the measurement of the interatomic distance more accurate. The double slit diffraction shows that the diffraction pattern is well resolved if the wavelength of the diffracting wave is smaller than the slit separation. In terms of LIED this condition relates the De Broglie wavelength of the electron $\lambda_{electron}$ to the atomic separation R_a:

$$\boldsymbol{\lambda_{electron} = \frac{h}{\sqrt{2m_eE}} \leq R_a,} \qquad (1)$$

where E is the kinetic energy of the electron at recollision. With simple classical arguments it can be shown that the maximum kinetic energy of the recolliding electron is $3.17U_p$ being U_p the so called ponderomotive potential:

$$\boldsymbol{U_p = \frac{e^2E_0^2}{8m_ec^2}\lambda_{field}^2.} \qquad (2)$$

Here E_0 is the amplitude of the electric field whereas λ_{field} is its wavelength. Combining eq. (1) and (2) we obtain the scaling of the electron De Broglie wavelength with the field wavelength:

$$\boldsymbol{\lambda_{electron} \propto \frac{1}{\lambda_{field}},} \qquad (3)$$

which shows that a clearer diffraction pattern is expected for longer wavelengths. For this reason the radiation produced by the TOPAS at Artemis is ideal as it reliably outputs short pulses (50 fs) with energy as high as 1 mJ at 1300 nm. The intensity is the other key aspect to take into account and it appears in the form of electric field amplitude in equation (2).

In order to observe a clear diffraction pattern the molecules should be aligned along a preferential direction in the lab frame. A random alignment of molecular sample with respect to the (ionizing) laser polarization is expected to cancel the diffraction pattern due the averaging on all possible orientations. Therefore, following the scheme outlined in ref. [5], a molecular alignment technique is employed in order to eliminate at least partially this effect. The experiment becomes then a pump-probe experiment in which a laser pulse (pump, 780 nm from Red Dragon) is employed to induce non-adiabatic molecular alignment and another laser pulse (probe, 1300 nm, the output of the TOPAs, delayed with respect to the pump) ionizes the sample.

In ref. [5] LIED was observed in simple diatomic molecules, such as N_2 and O_2. In the LIED experimental campaign the first objective was to confirm the validity of the technique and hence to record electron momentum distributions in aligned N_2 for comparison. The original plan included also a step forward in terms of molecular complexity: to observe LIED in a simple triatomic molecule such as CO_2.

Unfortunately LIED has not been demonstrated yet with the setup available at Artemis. As it will be explained in the last section this was due to the fact that the electron VMI images in LIED configuration turned out to be heavily affected by space charge. However important steps have been taken in that direction. The VMI has been commissioned and the first experiment, above threshold ionization (ATI) in N_2, has confirmed that the spectrometer is capable of detecting electrons with kinetic energies in the 0-200 eV range. Moreover a certain degree of molecular alignment has been obtained both in N_2 and CO_2. These preliminary results will be presented in the next two sections whereas a brief discussion on the space charge effect which affected the LIED measurements will be the subject of the concluding one.

Commissioning of the VMI: ATI ionization in N_2

An important preliminary part of the experiment is to confirm experimentally that the VMI spectrometer is capable to measure photoelectron spectra with kinetic energies ranging from nearly zero to 200 eV. SIMION simulations can in principle provide pixel-to-energy calibration curves which readily give the maximum detectable kinetic energy but it is always advisable to obtain an experimental calibration which accounts for all the possible stray fields which are inevitably neglected in simplified simulations. In this experiment the above threshold ionization (ATI) in N_2 was studied: the presence in the PES of peaks separated by the photon energy allows to perform a reasonably accurate calibration for lower voltages on the electrodes which can then be extrapolated to obtain an estimate of the pixel-to-energy conversion for high voltages.

Above threshold ionization [6] in atoms and molecules is a multiphoton process which occurs at intensities on the order of 10^{13} W/cm^2 and near infrared fields (780 nm). The intensity of the radiation is such that the atom absorbs a number n of photons above the minimum number required to overcome the potential barrier. As a consequence the excess kinetic energy spectrum of the released electrons presents peaks separated by the photon energy corresponding to absorptions of 1,2,3,etc. photons above the minimum required. The intensity in this regime is high enough to allow the absorption of multiple photons but the amplitude of the electric field is still insufficient to affect seriously the Coulomb potential and hence allow electrons to tunnel out. If I_p is the ionization potential the Keldish parameter γ defined as

$$\boldsymbol{\gamma = \sqrt{\frac{I_p}{2U_p}}}, \qquad (\mathbf{4})$$

allows to distinguish between the ATI regime and the tunneling regime according to the light intensity and wavelength. If $\gamma \ll 1$ tunneling ionization dominates whereas if $\gamma \geq 1$ we are in the ATI regime.

This does not imply that in the ATI regime the ionization potential is unaffected. In such an intense electromagnetic field I_p is expected to increase by an amount which is roughly equal to the ponderomotive potential. As the intensity increases the ATI peaks shift to lower energies (as I_p increase) but they also start to break into more complicated structures. These are called Freeman resonances because they are due to excited states (Rydberg) brought into resonance (with an harmonic of the laser field) by the AC shift.

With classical arguments it can be shown that the maximum kinetic energy that an electron gains in the laser field is $2U_p$. As a consequence a cut-off in the PES is expected around this value. However the ATI picture outlined so far does not take into account that even in the ATI regime an electron can be driven back on the parent ion when the field changes sign and then it can acquire further kinetic energy. Newton's law predict that the maximum kinetic energy for a rescattered electron is $10U_p$. Several experimental ATI spectra confirm this rescattering picture and show a clear plateau region ranging from $2U_p$ to $10U_p$.

The calibration of the VMI spectrometer was performed by acquiring images of electron VMI of randomly oriented N_2 molecules for different electrodes voltages. Nitrogen was delivered into the vacuum chamber by means of a continuous flow gasjet. The radiation coming from the Red Dragon at 780nm, 60fs with a pulse energy of the order of 100 μJ was focused down to a spot of 100 μJ diameter (estimated intensity in the low 10^{13} W/cm^2). Images were recorded at a repeller voltage ranging from 1 kV to 5 kV and the repeller/extractor ratio was kept constant at 0.72. Each image is the accumulation of 80000 laser shots. No background subtraction was performed as it was observed that when the jet was off the signal disappeared. In figure 1 a sample electron VMI image is shown. Electrons are preferentially ejected along the laser polarization

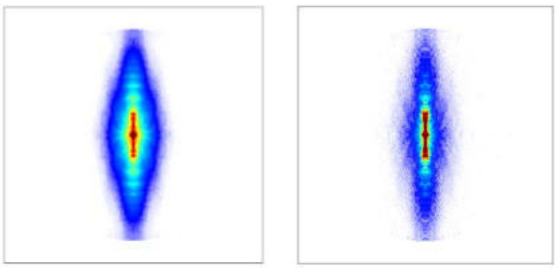

Figure 1: Sample VMI image of ATI in N_2 with 780 nm (intensity in the low 10^{13} W/cm^2). The voltage on the repeller was set to 1 kV and the extractor\repeller voltage ratio was 0.72. Raw image is shown in panel (a) and inverted (and symmetrized) image is shown in panel (b).

which is the vertical direction in the figure. The spectrum along this direction clearly presents a sequence of peaks which are expected to be separated by the photon energy. The angular distribution for energies below the first ATI order carries the signature of the Rydberg states brought into resonance by the shift in the ponderomotive potential. A very similar structure has been previously observed in atoms and other diatomic molecules [7].

The Abel inversion of the images has been performed with the iterative algorithm proposed in ref. [8]. Image (a) shown in fig. 1 is the output of the inversion after 100 iterations.

The radius-to-energy calibration is obtained by extracting the photoelectron spectrum along the laser polarization. The absolute energy corresponding to each peak cannot be assign accurately as it highly depends on the intensity of the laser which can be estimated only very roughly. However the distance between two adjacent peaks has to be equal to the photon energy so if p_n is the pixel position of the n-th peak then its energy has to follow the relation

$$E_n - E_0 = Ap_n^2 - Ap_0^2 \qquad (5)$$

where p_0 is the pixel position of the first ATI ring and $\boldsymbol{E_n - E_0 = n\hbar\omega}$. The values of A and p_0 can be obtained by means of a simple linear fit. The PES along the laser polarization in energy scale is shown in figure 2.

In order to detect electrons with kinetic energies in the range 0-200 eV the maximum voltage of 15 kV has to be applied to the repeller. A calibration at this voltage setting would be ideal but it is not possible to observe clear ATI rings in N_2 at those voltages because the image would be squashed into the central region of the MCP. The radial distributions along the laser

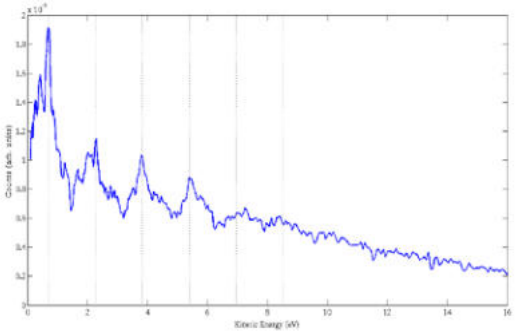

Figure 2: Excess kinetic energy spectrum of electrons in ATI of N_2 with 780 nm and intensity in the low 10^{13} W/cm^2. The spectrum has been extracted from the experimental image shown in fig. 1. The dotted vertical lines indicate the ATI peaks and are separated by the photon energy.

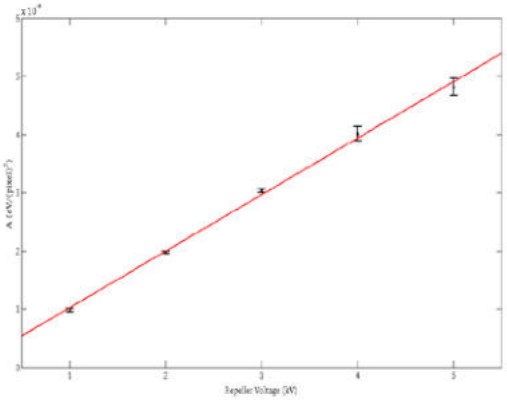

Figure 3: Linear fit of the pixel-to-energy calibration coefficient A_m as a function of the repeller voltage V_m.

polarization would be concentrated at very low radii and it would be impossible to resolve any structure.

The solution adopted here is based on the linear dependence of coefficient A in eq. (5) with the voltage. Images analogous to the one in fig. 2 were acquired for a repeller voltages V_m of m = 1,2,3,4,5 kV. For each image the value of the corresponding calibration coefficient A_m is determined. From a linear fit of A_m with respect to m (see fig. 3) the calibration coefficient at 15 kV A_{15} can be extrapolated.

Molecular alignment at Artemis

In the non-adiabatic molecular alignment technique [9] a linearly polarized femtosecond laser beam is focused on a sample of rotationally cooled molecules. For intensity on the order of 10^{12} W/cm^2 and for pulse durations on the order of 100 fs a rotational wavepacket is initially created during the interaction of the molecule with the beam which results in an alignment along the laser polarization. Because of the short pulse duration the phase relationship between the different components of the wavepacket is not destroyed (coherence is preserved) and after every rotational period (but also after every half of the rotational period) the alignment reappears (full revival or half revival). This technique has been widely used recently because it has the crucial feature of offering field-free alignment.

A certain degree of molecular alignment has been obtained at Artemis during the LIED campaign in both N_2 and CO_2. To obtain some rotational cooling a mixture of the sample gas in helium (5% for N_2 and 4.5% for CO_2) has been delivered to the AMO chamber by means of a continuous flow gasjet. A small fraction (30 μJ) of the linearly polarized output of the Red Dragon has been employed as the aligning laser beam and the degree of alignment has been probed by ionizing the sample with circularly polarized radiation from the TOPAS at 1300 nm. The momentum distribution (VMI image) of the ion fragments has been measured for different delays between the aligning and the ionizing pulses. From the plot of the mean value of $\cos^2\theta$ (θ is measured respect to the laser polarization) as a function of the delay the settings corresponding to alignment and anti-alignment has been clearly identified and degree of alignment has been estimated.

The ideal physical process that allows to measure accurately the degree of alignment is Coulomb explosion [10]. If the sample molecule is highly ionized (charge state equal or higher than 3) the dissociation happens very fast because of the Coulomb repulsion between the two positive ions. In this way the two fragments fly along the internuclear axis and their angular distribution can be taken as a reasonable measurement of the molecular alignment.

If the molecule is only ionized once or twice the dissociation happens via dissociative electronic states: after ionization the

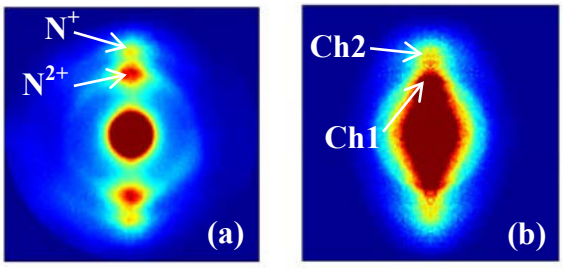

Figure 4: Ion VMI images of N_2 (a) and CO_2 (b). The dissociative channels are shown. The colour scale for CO_2 has been saturated to highlight the relevant features.

molecular ion is left in a highly excited electronic state that leads to dissociation. In this case the molecule can still undergo some nuclear motion before it fragments and therefore the momentum distribution is a less accurate measurement of the alignment prior to the ionization.

Ideally very high charge states are required to have a faithful measurement of the alignment. In this particular experiment due to limited energy in the 1300 nm beam and a non optimal focusing in the interaction region only up to N_2^{3+} has been detected in N_2 and up to CO_2^{2+} for CO_2. As a consequence the estimate of the degree of alignment given later in this section has to be considered as a lower limit of the real one.

Also the probe beam is capable of inducing alignment in the sample. Consequently a circularly polarized probe is often used in order to reduce this effect. In the data presented in the following the pulse energy for the probe beam is 330 μJ for N_2 and around 200 μJ for CO_2.

The detector has not been gated to select specific species. Each image is therefore a collection of all the molecular fragments. In case of N_2 we can clearly see two separate channels whose kinetic energies suggests that they are N^+ and N^{2+}. In case of CO_2 although the kinetic energy release spectrum presents two rather separate peaks the distribution is rather broad and therefore a clear identification of the peaks is not possible.

In fig. 4(a) a typical ion VMI image is shown for N_2 (accumulation over 4000 laser shots). The saturated spot in the middle of the image is due to low kinetic energy ions (such as N_2^{n+}). The first pair of spots (at lower radii) has a kinetic energy of roughly 4 eV which is the expected kinetic energy release of N^+ fragments. The outer pair corresponds to a kinetic energy of roughly 8 eV and it is assumed to be to due to N^{2+} [11].

The Abel inversion has been performed with iterative algorithm [8] on raw images which had been previously symmetrized with respect to the axis of cylindrical symmetry.

It can be shown that in case of impulsive alignment there is a revival of the alignment not only after every rotational period but also after every half of the rotational period. This further revival is commonly referred to as half revival. Since N_2 has a rotational period of 8.2 ps the half revival is expected around 4.1 ps so images have been taken around that value. For each image the quantity $\cos^2\theta$ has been calculated for the two channels. The results are shown in

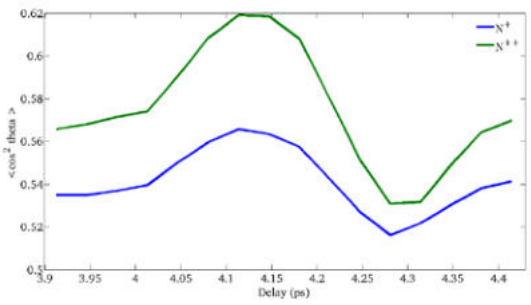

Figure 5: Half revival delay scan in N2

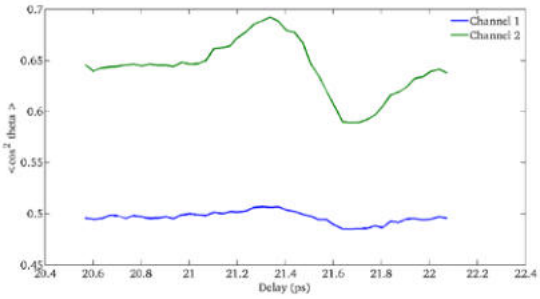

Figure 6: Half revival delay scan in CO_2

Simulations show that right after the half revival the relative phase of the rotational wavepacket adjusts so that there is the so called anti-alignment for which the molecules lie in a plane perpendicular to the laser polarization. In figure 5 we see first an increase of the value of $\cos^2\theta$ which is peaked roughly at half the rotational period (half revival). Right after that the value of $\cos^2\theta$ decreases abruptly. The lowest point corresponds to the anti-alignment.

The situation for CO_2 is less clear. In figure 4b a typical ion VMI image is shown. Since the detector was not gated each image is a collection of all positive fragments. Here different channels are not clearly distinguished in the image. However the KER distributions presents two peaks Due to the rather broad energy distribution and because of the higher complexity of the dissociation mechanisms in CO_2 compared to N_2 the identification of the peaks has not been possible. The clear circle which is present in the image is likely to be an artefact whose origin is still uncertain. A possible explanation is that it is a sort of image of the hole in either the extractor plate or the ground plate.

The rotational period of carbon dioxide is 42.7 ps so the half revival is expected around 21 ps.

From figure 5 and 6 it can be seen that the contrast between the values of $\cos^2\theta$ for the aligned sample and anti-aligned sample is very small. This seems to suggest that although some molecular alignment has been achieved the actual degree of alignment is not particularly high. The reason for this may be due a high rotational temperature of the gas sample when it is delivered in the gas chamber. As it has been stated earlier Coulomb explosion is the ideal tool to obtain a more realistic estimate of the degree of alignment. Further measurements are then required to investigate the real rotational cooling capabilities of the AMO endstation at Artemis.

High Kinetic Energy Electrons

After having established that with the current setup it is possible to achieve a certain degree of alignment and once the delay setting corresponding to alignment and anti-alignment has been found for N_2 and CO_2 the polarization of voltages on the electrodes have been switched to detect electrons.

Electron VMI images have been taken at different settings (alignment, anti-alignment, random alignment) for the delay between the pump beam (E=30 μJ λ=780 nm) and the probe beam (λ = 1300, various pulse energies). It was noticed that even for low intensities of the probe beam the electron distribution was extended over the whole detector. The repeller voltage was 15 kV and therefore electrons hitting the MCP around the edge were assumed to have energies above 200 eV. It was therefore assumed that the intensity was sufficient to induce rescattering at a De Broglie wavelength short enough to observe LIED.

Images were taken at different polarization configuration: both pump and probe parallel to the detector, pump parallel and probe perpendicular to the detector, pump perpendicular and probe parallel to the detector. In none of these cases a significant difference has been observed in the images between the aligned sample and the anti-aligned sample. A more careful

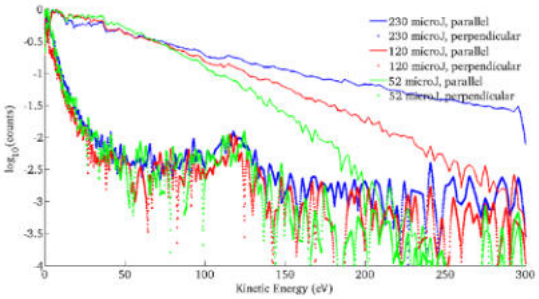

Figure 8: Parallel and perpendicular photoelectron spectra (see text) in N_2 obtained with different pulse energies (λ = 1300 nm).

offline data analysis has revealed that the reason for this lies in the fact that all the electron measurements were affected by space charge.

In figure 7 a set of N_2 photoelectron is shown for different pulse energies in the probe beam. The pump beam was also present but it was too weak to ionize independently and the delay was set to have a random alignment so its effect can be neglected. The polarization of both beams was parallel to the detector. The parallel PES is obtained by an angular integration over 20 degrees around the laser polarization. The perpendicular PES is obtained by integrating over 20 degrees around the horizontal direction.

A more careful estimate of the intensity shows that for a pulse energy of 230 μJ the intensity is on the order of $6 \cdot 10^{13}$ W/cm^2 which correspond to a ponderomotive potential of 8 eV. The maximum kinetic energy for recolliding electrons is $10U_p$ and hence no electrons should be observed at a kinetic energy higher that 80 eV. This is in sharp contrast with what is plotted in fig. 7. A possible explanation was that the images were highly affected by space charge. This seems to be confirmed by the fact that the cutoff in the perpendicular PES does not depend on the pulse energy. Moreover a $2U_p$ cut-off is expected in the parallel PES which indicates the maximum kinetic energy of direct electrons. This cutoff is not present in any of the experimental images.

Conclusions

In the very first experiment of the newly commissioned AMO end station at Artemis significant steps have been done toward LIED. The capability of detecting high kinetic electrons has been confirmed and a certain degree of molecular alignment in N_2 and CO_2 has been obtained.

Because of space charge LIED has not been demonstrated yet with the current setup. This can be easily fixed by reducing the gas density at the interaction region. However the acquisition time will have to increase significantly as rescattered electrons are expected to be several orders of magnitude lower in number than the direct ones.

Acknowledgements

The authors acknowledge the contribution of S. Hook, P. Rice, S. Spurdle and T. Strange (Central Laser Facility, STFC RAL) for the technical support.

References

1. L.D. Landau and E.M. Lifshitz, *Quantum Mechanics* (Pergamon, New York, 1965), 2nd ed., pg 276.
2. Y. Mairesse *et al.*, *Science* **302**, 1540 (2003).
3. T. Zuo *et al.*, *Chem. Phys. Lett.* **10**, 35 (2008).
4. M. Lein *et al.*, *Phys. Rev. lett. A* **66**, 051404 (2002).
5. M. Meckel *et alias*, *Science* **320**, 1478 (2008).

6. P. Agostini, F. Fabre, G. Mainfray and G. Petite, *Physical Review Letters*, **42**, 1127 (1979).

7. Y. Liu, X. Liu, Y. Deng, C. Wu, and Q. Gong, *IEEE JOURNAL OF SELECTED TOPICS IN QUANTUM ELECTRONICS*, **18**, 1 (2012).

8. M. J. J. Vrakking, *Rev. Sci. Instrum.* **72**, 4084 (2001).

9. H. Stapelfeldt and T. Seideman, *Rev. of Mod. Phys*. **75**, 543 (2003).

10. C. Ellert, H. Stapelfeldt, E. Constant, H. Sakai, J. Wright, D. M. Rayner and P. B. Corkum, *Phil. Trans. R. Soc. Lond. A* **356**, 1736, 329-344 (1998)

11. W. Guo, J. Zhu, B. Wang, Y. Wang and Li Wang, *Phys. Rev. Lett. A* **77**, 033415 (2008).

Exploring the onset of superfluid behaviour in quantum clusters using time-domain measurements

Contact *Klaus von Haeften (kvh6@le.ac.uk)*

Gediminas Galinis, Luis Guillermo, Mendoza Luna, Mark Watkins, Klaus von Haeften

Department of Physics and Astronomy
University of Leicester, UK

Andrew Ellis

Department of Chemistry
University of Leicester, UK

Russell Minns

Department of Chemistry
University of Southampton, UK

Edmond Turcu, Cephise Cacho, Emma Springate

Central Laser Facility
Rutherford Appleton Lab, UK

Introduction

Many features of superfluidity can be broadly described in terms of the absence of friction. In 1946 Andronikashvili investigated the interaction of rotating objects with superfluid helium using a torsional pendulum that consisted of several stacked disks. When immersed into liquid helium the speed of rotation was found to slow down, as one would expect for a classical liquid which follows the rotation of the disks and effectively increases their moment of inertia. He then cooled the helium below the superfluid phase transition at 2.18 K and observed that the speed of rotation began to change: this time the speed of rotation increased as if the effective moment of inertia of the disks became smaller. The increase of the rate of rotation continued to a temperature of 1 K, an observation that was interpreted as the gradual establishment of superfluidity; in other words, a normal-fluid and a superfluid phase coexisted in a specific ratio that depended on the temperature.

The 'Andronikashvili-Experiment' confirmed London's two-fluid model of superfluidity but it did not reveal any insight into the underlying processes at a microscopic level, nor did it permit the study of dynamical effects in a molecular time frame. Undertaking an investigation at the microscopic level would have required Andronikashvili's disks be replaced with molecules, but introducing molecular probes is very difficult because all foreign molecules would freeze at the vessel walls or aggregate into clusters at the low temperature of liquid helium.

Helium droplet beams provide a solution to this problem. Superfluid helium droplets can be generated in supersonic expansions of helium gas at low temperatures and high pressures through a tiny nozzle. The droplets fly through vacuum and when collisions with molecules occur the molecules become trapped inside them. This process is selective and one can tune the gas density so that on average precisely one single molecule is 'picked-up' and dispersed in a superfluid droplet.

Here, we have employed the helium droplet method to probe molecular interactions in superfluids. Our aim is to investigate the size dependence, *i.e*. to explore how many helium atoms are needed to produce evidence of superfluidity. A further aim is to investigate how slow or fast rotating molecules respond to a superfluid environment. To deliver this ambitious aim, which is essentially a molecular version of the Andronikashvili experiment, we apply an entirely new method to obtain this information: we excite rotational wavepackets of single molecules in superfluid helium and study how these wavepackets propagate in time. This will directly show how the rotational speed is affected by a potential superfluid environment and it will also show how local superfluids, in close proximity to a molecule, respond to instantaneous rotational excitation.

Experimental

The first experiments were performed at the Artemis beamline at the Central Laser Facility (CLF) using the AMO chamber. To create rotational wavepackets we used the method of non-adiabatic alignment. Short and intense 800 nm laser pulses of typically 30 to 900 fs pulse width and 1 mJ energy were fired onto molecules in helium clusters. These photons interacted with the molecules non-resonantly and created rotational wavepackets through sequential excitation and de-excitation of rotational levels in Raman-type cycles (figure 1). The wavepackets propagated in time and the state of alignment was probed after a set time delay. A schematic of the experimental set-up is shown in figure 2.To achieve high time resolution it was important to probe the state of alignment almost instantaneously and this was achieved by firing intense *probe laser* pulses of 30 fs in length onto the molecules, which subsequently disintegrated via so-called Coulomb explosion and ejected the fragments in opposite directions. The velocity vectors of the fragments were measured using a velocity map imaging (VMI) spectrometer and their angular distribution was evaluated as a function of the delay time. Using this technique it was possible to track the phase of rotational motion over many rotational periods. A specific advantage of this technique is that wavepackets containing a variable number of rotational levels can be 'constructed' [1], allowing the study of the response of the environment to different speeds of rotation. A second advantage is that the resolution increases with the number of rotational cycles detected.

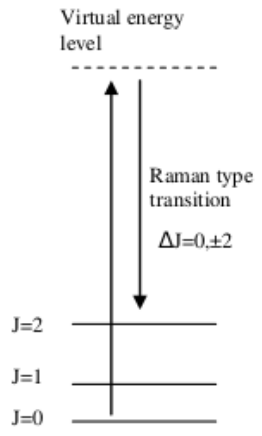

Figure 1: Schematic showing the sequential excitation and de-excitation of rotational levels in Raman cycles.

Instead of making helium droplets, these experiments used very small helium clusters in order to identify incipient molecular superfluidity. Molecule-doped helium clusters were produced in a slightly modified fashion in which a mixture of helium gas and molecules in low concentrations were co-expanded into vacuum. An advantage is that the nozzle only needs to be moderately cooled. To maximize throughput a cluster source (provided by the University of Leicester) comprising a pulsed nozzle of the Even-Lavie design was employed [2].

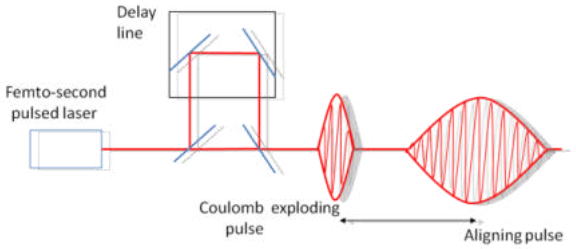

Figure 2: Schematic of the experimental set-up.

Results

The first tests were undertaken using CO as the probe molecule. CO is a good benchmark system because its rotational motion has previously been investigated in small clusters consisting of up to 8 helium atoms using frequency-domain spectroscopy [3]. Large helium droplets doped with CO have also been investigated [4]. While the well-known rotational frequencies of small doped clusters are an excellent benchmark our investigation aimed to explore the range from 9 to 1000 helium atoms because in this size range coupling between rotational motion and collective excitations, such as phonons, are expected to emerge. For CO the coupling to phonon excitations is expected to be particularly strong. Also, measurements of the rotational frequencies of CO in the previous frequency-domain-based investigations in large helium droplets were restricted by certain underlying assumptions. With the new approach more accurate results should be achievable.

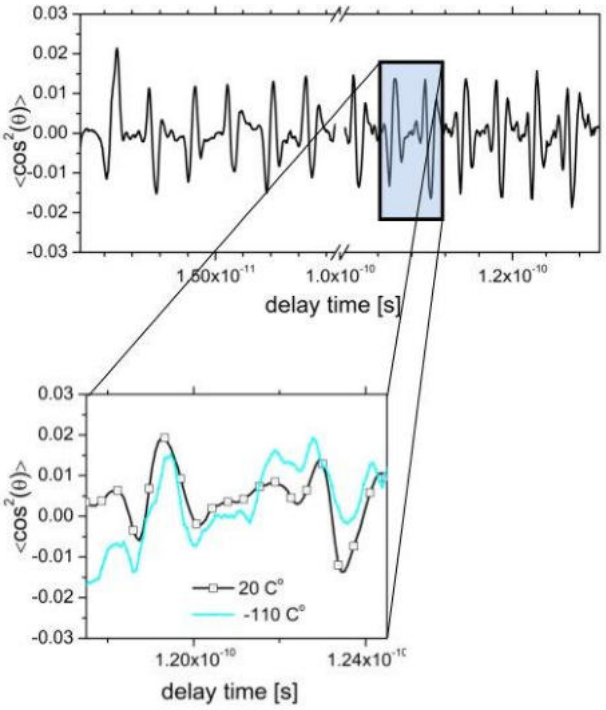

Figure 3: Trace of the angular asymmetry of fragment velocities representing the propagation of rotational wavepackets. The sharp lines represent full and half 'revivals', where the amplitude and phase of the wavefunction assumes its original value. The inset shows two traces for two different expansion conditions. At a nozzle temperature of -110^0 C clusters form and a feature matching the rotational speed of previously measured CO-He$_5$ appears. This correlation proves that our concept works.

Figure 3 shows the angular asymmetry of O^{++} and C^{++} fragments as function of the time-delay between alignment and probe laser pulses. The features show a periodicity that reflects the rotation of CO molecules. *This is the first time such rotational revivals have been seen in molecule-doped helium clusters.* 'Full revivals' occur at times t=1/2B where B is the rotational constant. When the cluster source was cooled to -110^0 C additional features emerged, as can be seen in the inset. These features were attributed to clusters of CO molecules and 5 helium atoms, which rotate more slowly and whose rotational frequency was known from previous microwave spectroscopy experiments [3].

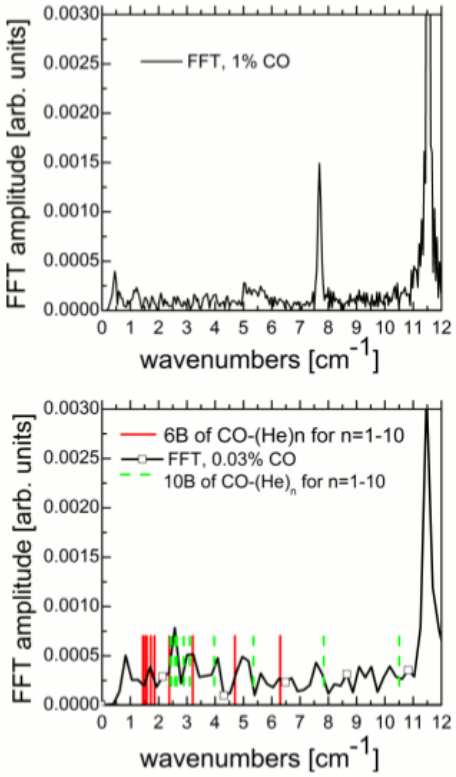

Figure 4: Fourier transform of the time-dependence of angular asymmetry of fragment velocities for two different CO concentrations. For expansions using 1% CO in helium the spectrum is dominated by molecular features. For 0.03% CO in helium additional features appear at low frequencies that cannot be assigned to *pure* CO. These frequencies match the rotational frequencies of CO molecules attached to small helium clusters previously measured using frequency domain microwave spectroscopy (stick spectrum).

Figure 4 shows Fourier transforms of the angular asymmetry traces for two different supersonic expansion conditions. The upper panel shows spectra where gas mixtures of 1% CO in helium were expanded whereas the lower panel shows spectra of expansions of concentrations of 0.03% CO in helium. Both spectra differ. The low-concentration spectrum shows a set of peaks at frequencies distinctively smaller than that of CO. These peaks match the positions of the previously determined frequencies of clusters of CO and up to 8 helium atoms. However, there are no peaks in the current work which match the frequencies of CO-He$_9$ and CO-He$_{10}$. Also, the high concentration spectrum shows features relating to the frequency at 10B of CO, which is absent for lower concentration. The pump laser conditions have not changed and these differences show that different molecular wavepackets establish, depending

on the expansion conditions. The specific reason for the difference is presently not understood but might be related to rotational cooling of the CO molecules. The cooling rate of our source is particularly high and we anticipate that we can generate beams in which the vast majority of CO molecules are in the rotational ground state.

Conclusions

Our experiments show that is possible to track the propagation of rotational wavepackets in helium clusters using the method of non-adiabatic alignment. The frequencies obtained for small CO-doped helium clusters match the benchmark data, which is highly encouraging. More data are needed to interpret features that deviate from predictions. These first experiments have established the experimental conditions required and have shown the feasibility of following the rotational motion of molecule-doped helium clusters in the time domain and now offer many exciting possibilities in the study of molecular superfluidity.

References

1. A. Przystawik, A. Kickermann, A. Al-Shemmary, S. Dusterer, A. M. Ellis, K. von Haeften, M. Harmand, S. Ramakrishna, H. Redlin, L. Schroedter, M. Schulz, T. Seideman, N. Stojanovic, J. Szekely, F. Tavella, S. Toleikis, T. Laarmann, Phys. Rev. A 85, 052503 (2012).
2. U. Even, J. Jortner, D. Noy, N. Lavie, and C. Cossart-Magos, J. Chem. Phys. 112, 8068 (2000).
3. A. Surin, A.V. Potapov, B.S. Dumesh, S. Schlemmer, Y. Xu, P.L. Raston, and W. Jager, Phys. Rev. Lett. 101, 233401 (2008).
4. K. von Haeften, S. Rudolph, I. Simanovski, M. Havenith, R. E. Zillich, and K. B. Whaley, Phys. Rev. B 73, 054502 (2006).